ORIGINAL PAPER

P. Galli · V. Bosi · S. Piscitelli · A. Giocoli · V. Scionti

Late Holocene earthquakes in southern Apennine: paleoseismology of the Caggiano fault

Abstract Although southern Apennines are characterized by the strongest crustal earthquakes of central-western Mediterranean region, local active tectonics is still poorly known, at least for seismogenic fault-recognition is concerned. Research carried out in the Maddalena Mts. (southeast of Irpinia, the region struck by the $M_w = 6.9$, 1980 earthquake) indicates historical ruptures along a 17-km-long, N120° normal fault system (Caggiano fault). The system is characterized by a bedrock fault scarp carved in carbonate rocks, which continues laterally into a retreating and eroded smoothed scarp, affecting the clayey-siliciclastic units, and by smart scarps and discontinuous free-faces in Holocene cemented slope-debris and in modern alluvial fan deposits. The geometry of the structure in depth has been depicted by means of electrical resistivity tomography, while paleoseismic analysis carried out in three trenches revealed surface-faulting events during the past 7 ky BP (^{14}C age), the latest occurred in the past 2 ky BP (^{14}C age) and, probably, during/after slope-debris deposition related to the little ice age (~1400–1800 A.D.). Preliminary evaluation accounts for minimum slip rates of 0.3–0.4 mm/year, which is the same order of rates estimated for many active faults along the Apennine chain. Associated earthquakes might be in the order of $M_w = 6.6$, to be compared to the historical events occurred in the area (e.g., 1561 and 1857 p.p. earthquakes).

Keywords Paleoseismology · Active tectonics · Historical seismicity · Seismic hazard · Italy

P. Galli (✉) · V. Bosi · V. Scionti
Civil Protection Department, USSN, Rome, Italy
E-mail: paolo.galli@protezionecivile.it

S. Piscitelli · A. Giocoli
CNR, Institute of Methodologies for Environmental Analysis,
Potenza, Italy

Introduction

Southern Italy is the most seismically active and hazardous zone of the central-western Mediterranean region, with shallow $M \geq 6.5$ earthquakes, which have always had a catastrophic impact on the highly vulnerable old-town centers. Whereas the strongest events occur in the toe of the Italian "boot" (i.e., $M \geq 7$ earthquakes of Calabria; return time 1–1.5 ky, Galli and Bosi 2002, 2003a), the highest frequency for $6.5 \leq M \leq 7$ earthquakes belongs to the area centered around the Irpinian Apenninic chain. Several villages of this region have been destroyed and rebuilt 5–6 times in the past 1 ky, last time after the November 23, 1980 $M_w = 6.9$ event (~3,000 casualties). Some of these earthquakes have roughly the same epicenter (i.e., they share the same seismogenic fault system; Fig. 1), whereas others overlap only the edges of their mesoseismic area (i.e., they are caused by different, conterminous structures).

In this paper we focus on the region located immediately SE to Irpinia, and in particular on the northern sector of the Maddalena Mts. (Figs. 2–3). This area has been struck by two disruptive earthquakes in 1561 and 1857, but it is not characterized by conclusive geological evidence as far as active tectonics is concerned. Actually, the gap in seismogenic fault-recognition interests wide sectors of the southern Apenninic chain, from the carbonate massif of Matese to the N (N-Matese fault: Galli and Galadini 2003) to the carbonate massif of Pollino to the S (Pollino fault: Michetti et al. 1997; Cinti et al. 2002; Figs. 1, 2a). In contrast to the central Apennines (e.g., Galadini and Galli 2000; Roberts et al. 2003), apart from the deep structural complexity of the inherited fold-and-thrust belt chain, this trouble in identifying active faults is mainly due to the high erodibility of the siliciclastic units forming the surface structure of the seismogenic belt, which do not allow the preserving of short-term, low-rate (< 1 mm/year) tectonic indicators (e.g., fault scarps).

Thus, results coming from the identification and trenching of a 17-km-long normal fault (Caggiano fault,
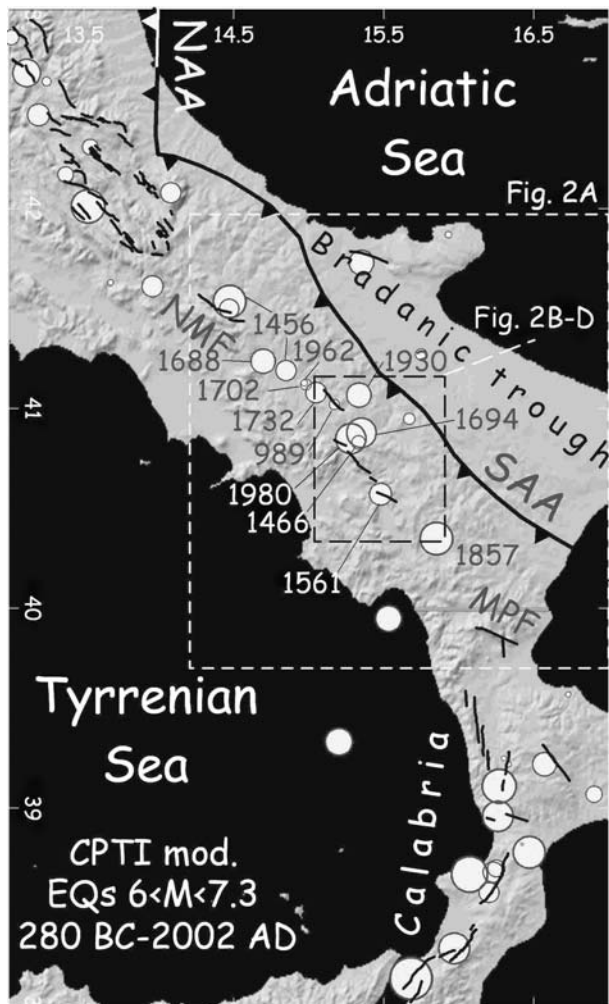
Fig. 1 Distribution of $M > 6$ seismicity in central-southern Italy (CPTI 1999, modified). *Bold lines* are known seismogenic faults (after Galadini and Galli 2000; Galli and Bosi 2002, 2003a, b); *NAA* northern Apenninic arc, *SAA* southern Apenninic arc, *NMF* northern Matese fault, *MPF* Mt. Pollino fault. The Irpinia region is located around the 1962–1930–1980 epicenters

CF from now Figs. 2, 3), located southeast of the Mt. Marzano fault system (MFS; i.e., the 1980 seismogenic structure), and new data on the historical earthquakes generated by this former fault, add another *tessera* to the seismotectonic knowledge of this sector of southern Apennine. Paleoseismic data are critical to both deterministic and probabilistic seismic-hazard analyses, wherein faults, on the basis of the story of their past ruptures, are evaluated as to their potential for generating future earthquakes of a given magnitude and within a given time period.

Seismotectonic framework of the area

The Apennines are a fold and thrust belt chain developed within the Africa–Adria–Europe relative plate motion. Their southern sector basically consists of a buried duplex system of Mesozoic–Tertiary carbonate thrust sheets overlain by a thick pile of rootless nappes derived from platform and basin depositional realms (Fig. 2a). Since the Neogene and during Quaternary times, the growth of the belt was driven by (1) the westward Ionian lithosphere subduction, (2) flexural-hinge retreat of the Adriatic foreland, and (3) contemporary back-arc extension of the Tyrrhenian basin (Patacca and Scandone 1989). According to Cinque et al. (1993), the frontal thrust sheet of the Southern Apenninic Arc migrated diachronously eastward. In its northern sector (NAA in Fig. 1) it has been sealed by early Pleistocene marine sediments, while in the southern sector, early Pleistocene deposits are instead involved in compressional deformation (late Middle Pleistocene in the Bradanic trough; SAA in Fig. 1, Pieri et al. 1997). Since 0.7–0.5 My ago, also due to the Adria plate NNW drift and rotation (Meletti et al. 2000; Devoti et al. 2002), the chain has been affected by NE–SW extension, with the largest deformations, earthquakes, and evidence of active normal faulting mainly concentrated along the axial belt (e.g., Galadini and Galli 2000; Fig. 1).

Overview of the regional seismicity and indication of active tectonics

Besides the strong shaking and damage induced by $M > 6.5$ conterminous Apenninic earthquakes (e.g., December 1456, Magri and Molin 1979; September 1688, Boschi et al. 1997), the investigated region has been the epicentral zone of at least nine $M > 6$ events in the past 1 ky, six of them being clustered in the last three centuries (one every ∼50 years, on average). They are the 989, 1466, 1561, 1694, 1702, 1732, 1857, 1930, 1962, and 1980 events (see epicentral locations in Fig. 1). At least two of these (the 1466 and 1694 earthquakes) have roughly the same epicentral area as the 1980 event, and their effects are summarized in the next paragraphs, together with the 1561 and 1857 events. The others occurred all NW of the 1980 EQ, the closest being the 989 and 1732 events. Instrumental seismicity recorded in the past years (Frepoli and Amato 2000) consists of shallow crustal hypocenters (upper 15 km), mainly related to NW–SE normal or E–W strike-slip faults.

The January 14, 1466 earthquake

This event, although reported by Postpischl (1985; Io = 7 MCS), Baratta (1901) and Bonito (1691), has been omitted in all the current Italian seismic catalogues (Camassi and Stucchi 1996; Boschi et al. 1997; Working Group CPTI 1999; CPTI from now). Its scant seismological standing is probably due to the shadow effect caused by the catastrophic 1456 earthquake(s), the fame of which "obscured" other near events, deceiving many authors, as stressed since Bonito (1691) time. Actually,
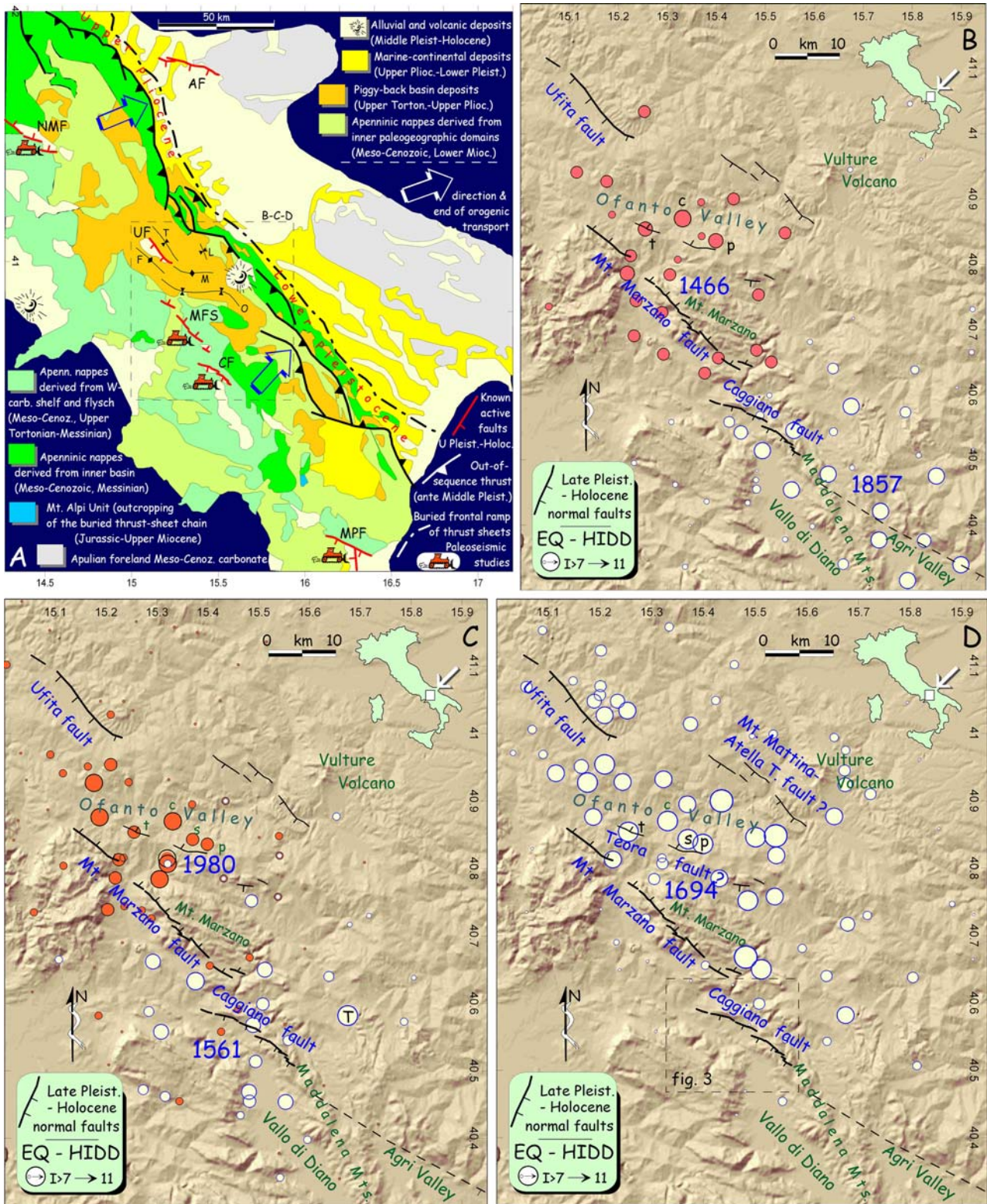
Fig. 2 a Structural map of southern Italy showing known active faults (the *bulldozer* indicates faults studied by means of paleoseismological studies); *AF* Apricena fault (Patacca and Scandone 2004); *NMF* northern Matese fault (Galli and Galadini 2003); *UF* Ufita fault (Brancaccio et al. 1981); *MFS* Mt. Marzano fault system (Pantosti et al. 1993); *CF* Caggiano fault (Galli and Bosi 2003b); *MPF* Mt. Pollino fault (Cinti et al. 1997; Michetti et al. 1997). **b, c,**
d Highest intensity data points distribution (HIDD) of the 1466, 1561, 1694, 1857, and 1980 earthquakes (EQ). Note that the 1466, 1694, and 1980 events share a large part of their HIDD. In particular, the 1466 and 1980 HIDD suggest a partially common seismogenetic structure (MFS), as 1561 and northern-1857 HIDD (CF). See location of these frames in Fig. 1. *Dashed frame* in **d** is the studied area

Table 1 Intensity datapoints of the poorly known, January 14, 1466 earthquake. This unpublished list consists of 29 localities the intensities of which has been evaluated in terms of Mercalli Cancani Sieberg (MCS) scale (Galli 2003)

Lon	Lat	I MCS	Location
15.331	40.87	10	Conza della Campania
15.218	40.786	9–10	Calabritto
15.399	40.836	9–10	Pescopagano
15.255	40.854	9–10	Teora
15.512	40.65	9	Balvano
15.376	40.633	9	Buccino
15.435	40.9	9	Calitri
15.225	40.813	9	Caposele
15.289	40.726	9	Colliano
15.305	40.784	9	Laviano
15.486	40.753	9	Muro Lucano
15.232	40.69	9	Oliveto Citra
15.292	40.662	9	Palomonte
15.236	40.744	9	Quaglietta
15.482	40.668	9	Ricigliano
15.54	40.848	9	Ruvo del Monte
15.404	40.656	9	San Gregorio Magno
15.176	40.927	9	Sant'Angelo dei Lombardi
15.115	40.941	9	Torella dei Lombardi
15.253	41.034	9	Vallata
15.058	40.735	8	Acerno
15.369	40.895	8	Cairano
15.187	40.876	8	Lioni
15.37	40.843	8	Sant'Andrea di Conza
15.321	40.807	8	Santomenna
15.107	40.665	7	Campagna
14.26	40.855	6	Napoli
14.367	41.177	5	Caiazzo
14.529	40.926	5	Nola

Fig. 3 Shaded relief map of the investigated area (from a 20-m-spaced DEM derived from original 1:25.000 topographic data, courtesy of Istituto Geografico Militare, aut. 5410 of 6/6/2001). Trenches, topographical profiles (TP), and ERT location are shown. *MSGF* Mt. San Giacomo fault, *TF* Timpe fault, *TB* Timpa del Vento basin, *VB* Campo di Venere basin. Inset **a** shows the morphological trace of both MSGF and TF scarp. See location of this frame in Fig. 2d

the known historical accounts summarized recently by Figliuolo and Maturano (1996), coupled with other few unpublished coeval sources, but with scores of archeoseismic indication found in the investigated area (Galli 2003), makes it possible to trace a highest intensity data point distribution (HIDD, Table 1 and Fig. 2b; 29 localities) for this earthquake. In short, the evaluated MCS epicentral intensity is Io = 9.5 (I_{max} = 10), with an equivalent macroseismic magnitude ($M_e \cong M_w$) obtained by using the Boxer program (Gasperini 2002) of M_e = 6.5. As for the epicentral area, it could be observed that the author of one of the main historical sources (in Corpus Chronicorum Bononiensium 1940) described the earthquake effects by following a "spiral route" centered among the villages of Conza, Teora, and Pescopagano (C, T, and P in Fig. 2b). This zone fits to the 1980 macroseismic epicenter, whereas the two macroseismic epicenters differ by less than 5 km (1466: 15.33 E, 40.83 N; 1980: 15.28 E, 40.85 N). The strong similarity between the 1466 and 1980 earthquakes (in terms of HIDD and magnitude) proves that they were caused by the same seismogenic structure, i.e., the MFS. Although not recognized by Pantosti et al. (1993) in the paleoseismological analyses performed across the fault (the earthquake was completely unknown and unexpected at that time), the 1466 event could have, in our opinion, left its trace in their trench 1 (see Fig. 3 of Pantosti et al. 1993). In fact, this could be shown by the thickening of lower unit A in the
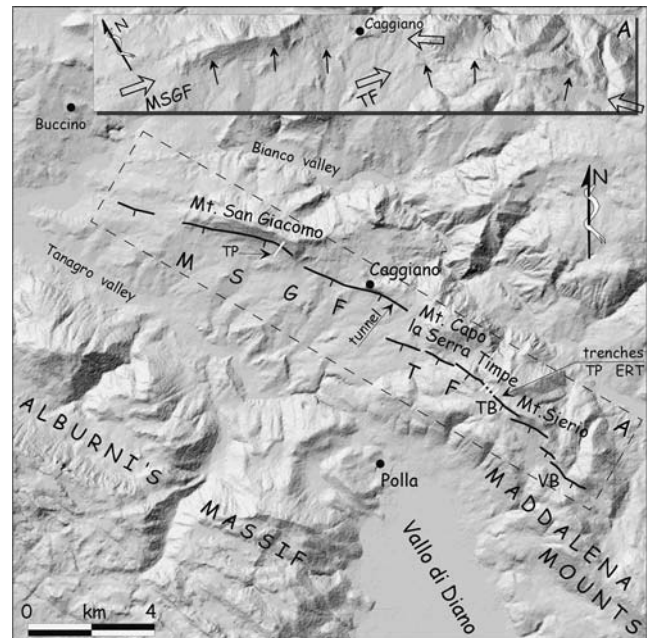
hanging wall, i.e., due to faulting (i.e., warping) occurred after 1392–1491 A.D. (^{14}C cal. age of sample 1A10) and before 1451–1643 A.D. (sample 2B3).

The September 8, 1694 earthquake

This is the strongest event to have struck Irpinia in historical times (Io = 10.5, M_e = 6.9, ~6,000 casualties, to be compared to the ~3,000 of 1980). It was preceded by two strong shocks (at the NW and SE tips of the mesoseismic area; Galli 2003) in 1680 (November 11, Io = 9) and 1692 (March 4, Io = 8.5). Figure 2d shows the HIDD evaluated for the 1694 event. Similarly to the 1466, also the epicenter of this event falls north of the Mt. Marzano carbonate massif, within an area characterized by the lack of clear evidence of active tectonics. If any, they are hidden in the siliciclastic deposits of the Ofanto valley, or they could fit with two faint indications which we saw in 1950s aerial photos: (1) discontinuous traces of N110° fault scarps, which are carved in the few carbonate rocks cropping out from the terrigenous units along the southern slope of the Ofanto valley, between Pescopagano and S. Andrea di Conza, and in the silicoclastic rocks near Teora. They alternate with vast landslides, earth flows, and solifluction, many of which activated or reactivated during the 1694 and 1980 events. The location of this N-facing scarp seems to fit with the description of the 10-mile-long (~16 km)

Table 2 Intensity datapoints of the cumulated effects of the July 31 and August 19, 1561 events. The lists consists of 36 localities the intensities of which has been re-evaluated in terms of Mercalli Cancani Sieberg (MCS) scale by Galli (2003). Former compilations (see in working Group CPTI (1999) contains 30 localities, with intensities differing in the range of 0–2 MCS degrees

Lon	Lat	I MCS	Location
15.675	40.582	10–11	Tito
15.376	40.633	10	Buccino
15.553	40.454	9–10	Atena Lucana
15.512	40.65	9–10	Balvano
15.489	40.568	9–10	Caggiano
15.292	40.662	9–10	Palo
15.481	40.469	9–10	Sant'Arsenio
15.308	40.558	9–10	Sicignano degli Alburni
15.486	40.752	9	Muro Lucano
15.494	40.514	9	Polla
15.482	40.455	9	SanPietro al Tanagro
15.508	40.599	9	Vietri di Potenza
15.316	40.462	8–9	Ottati
15.273	40.472	8–9	Pantoliano
15.638	40.64	8–9	Picerno
15.284	40.588	8–9	San Licandro
15.558	40.545	8–9	SantAngelo le Fratte
15.653	40.877	8	Atella
15.107	40.665	8	Campagna
15.786	40.573	8	Pignola
15.596	40.398	8	Sala Consilina
15.542	40.342	8	San Giacomo
15.464	40.434	8	San Rufo
15.321	40.807	8	SantoMenna
14.835	40.919	7–8	Atripalda
15.717	40.73	7–8	Avigliano
15.538	40.758	7–8	Bella
15.435	40.9	7–8	Calitri
15.431	40.785	7–8	Castelgrande
15.805	40.638	7–8	Potenza
15.679	40.717	7–8	Ruoti
15.541	40.819	7–8	San Fele
14.791	40.914	7	Avellino
14.765	40.679	7	Salerno
14.777	41.129	5	Benevento
14.260	40.855	5	Napoli

fracture mentioned in Vera e distinta relazione (1694; Teora fault in Fig. 2d). (2) On the N-side of the Ofanto basin, a ~20-km-long, N130° system of en echelon fault scarp-remnant (Mt. Mattina-Atella torrent fault in Fig. 2d; MAF) affects the Pliocene and infra-Pliocene terrigenous units, inducing topographic inversion on NE-facing slopes. These features are aligned with the N130° Ufita fault which, according to Brancaccio et al. (1981) and Basso et al. (1996) cuts late Pleistocene–Holocene deposits. Actually, the 1694 earthquake was apparently stronger than the 1980 one, although cumulate damage from the 1680, 1688 ($M_e = 6.7$, Fig. 1), and 1692 shocks might have "enlarged" its effects at the borders. Observing its HIDD (Fig. 2d) and considering that a $M = 6.9$ event would require a ~40-km-long normal fault, a reasonable hypothesis is that it was caused by the sub-contemporaneous rupture of the MAF (~20 km) and of another 20-km-long fault, which could be tentatively associated to the Ufita fault. Azimuthal damage distribution would be explained by a

SE directivity, whereas surficial breaks observed along the Teora slope could be interpreted as antithetic faulting. On the other hand, the hypothesis of a double event is strengthened by several contemporary sources (e.g., Vitale 1695), which explicitly speak of two separate shocks.

The November 23, 1980 earthquake

This earthquake ($M_s = 6.9$, Io = 10; CPTI 1999) has been investigated by several authors (e.g., Boschi et al. 1993). The earthquake was caused by a complex normal fault (Westaway 1996), mainly composed by 3–5 N310° segments, (main shock and 20-s sub-event), and by an antithetic fault SW-dipping (40-s sub-event; Bernard and Zollo 1989). The rupture nucleated at ~10 km depth (Amato and Selvaggi 1993) and caused ~35 km discontinuous surface faulting along the MFS (Cinque et al. 1981; Westaway and Jackson 1987; Pantosti and Valensise 1990). According to Bernard and Zollo (1989) and Westaway (1996) the main shock rupture propagated toward the NW. Directivity-induced effects related to normal faulting have been observed and inferred in several case histories in Italy (e.g., Galli and Galadini 1999), and during the 1980 event they would explain the stronger damage in the NW sector of the hanging wall, with respect to the SE one. This is evident in Fig. 2c, which shows both the 1980 HIDD (Monachesi and Stucchi 1997) and the Mt. Marzano fault.

The July 31 and August 19, 1561 earthquakes

These events are reported by all the seismic records starting from Pacca (1563), although Pacca's manuscript is the only main contemporaneous source for all the following writers. This fact has always limited the evaluation of reliable parameters (see also Castelli 2003. Io = 9.5, $M_e = 6.5$ in CPTI 1999). The recovery of dozen of unpublished contemporary notes, implemented with archeoseismic data and epigraphic indication found in the investigated area (Galli 2003), has allowed the refining of the HIDD (Table 2) and of the earthquake parameters. According to these data, the epicentral intensity is Io = 10 ($I_{max} = 10.5$) and the Boxer-derived equivalent macroseismic magnitude is $M_e = 6.7$ (cumulated value for the two "indivisible" shocks; epicenter 15.479E, 40.572N). Notwithstanding the high damage level, since both events were before sunset (the peasants were working in the fields), the earthquakes caused "only" 600 casualties. Figure 2c shows the HIDD (36 localities) of the earthquake, which appears to be centered around the CF (the high intensity of Tito, T in Fig. 2c, has been explained in terms of local amplification by Mucciarelli et al. 1999). This fault has been investigated in this work and will be discussed in detail in the following chapters.

The December 16, 1857 earthquake

This earthquake (Io = 10.5, M_e = 7; CPTI 1999) struck disastrously in the northern Vallo di Diano and Agri valley, causing between 10,000 and 20,000 casualties. Two main shocks occurred separated by a 3–4 min interval (Baratta 1901; Magri and Molin 1979) the first one felt mainly in the northern part of the mesoseismic area (Branno et al. 1983). This earthquake is known worldwide through the Mallet's (1862) pioneering seismological account. Figure 2b shows the partial (northern) HIDD, which could partly represent the effect of the first shock, falling around to the CF. Although several indications of surficial breaks were reported by the 1857 earthquake eyewitnesses, the scientific debate concerning the nature (normal or transcurrent fault? Blind or surface fault?), location (SW or NE dipping? SW side or NE side of the Agri valley?), and trend of the seismogenic structure responsible for this event is still open and various (e.g., Pantosti and Valensise 1990; Benedetti et al. 1998; Cello et al. 2003). As far as deformations of ^{14}C-dated deposits, only Giano et al. (2000a, b) point out post-20-ky faulting in the northern Agri Valley, along a NS high-angle transpressional fault (western slope of Maddalena Mts).

Geology of the investigated area

The Maddalena Mts. (1503 m a.s.l.) are the southeastern continuation of the carbonate massif of Mt. Marzano (Fig. 2). They extend from NW to SE over 50 km, separating the Quaternary intermontane lacustrine basin of Vallo di Diano (Ascione et al. 1992; 450 m a.s.l.) to the west from the high Agri valley basin (580 m a.s.l.; Giano et al. 2000a, b) to the east. The main ridge is built up by

Triassic dolomites, Jurassic and Cretaceous carbonate breccias, and Cretaceous–Paleogenic saccharoidal limestones (Maddalena Mts. Unit, sensu Ippolito et al. 1975), stratigraphically overlapped by Miocene carbonate-siliciclastic deposits (Sierio Formation) and by the arenaceous Castelvetere Flysh (Pescatore et al. 1970). Although not reported on the official cartography, thin strip of upper Pliocene sand and clay are preserved in few intermontane depressions (Lucchetti 1943). The entire carbonate ridge is superposed onto the Lagonegro basin units (Scandone and Bonardi 1968).

Its northern sector is bounded on the western slope by a NW–SE normal faults system, the CF being the northernmost and, in our opinion, presently active segment. This fault is composed by two en echelon main strands, showing a right step south of the Caggiano village: the Mt. San Giacomo and the Timpe faults (Fig. 3).

Mt. San Giacomo fault

This N110° northern strand of the fault system is 9-km long and displays a spectacular rock fault scarp, carved for more than 3 km along the Cretaceous carbonate of the SW flanks of Mt. San Giacomo (Fig. 4b). The latter presents a typical planar slope (*sensu* Parsons 1989), which followed a "Lehmann" slope replacement evolution (i.e., scarce basal removal; Young 1972). The fault scarp has been described since Brancaccio et al. (1978, see also Ascione et al. 1992), being interpreted by these authors both due to exhumation and to recent tectonic motion. According to Ascione et al. (1992), the uplift of the Mt. San Giacomo ridge (970 m a.s.l.), which separated the basins of the Tanagro and Bianco rivers (Fig. 3), was driven along N120° faults after the

Fig. 4 Topographical profiles along the Serra San Giacomo (**a**) and Timpa del Vento (**c**) SW slopes (benchmarks every 1 and 0.5 m, respectively). **b** and **d** are view looking N of the fault scarps (*arrows*) of Monte San Giacomo and Timpa del Vento (**a** and **c** are the location of the profiles)
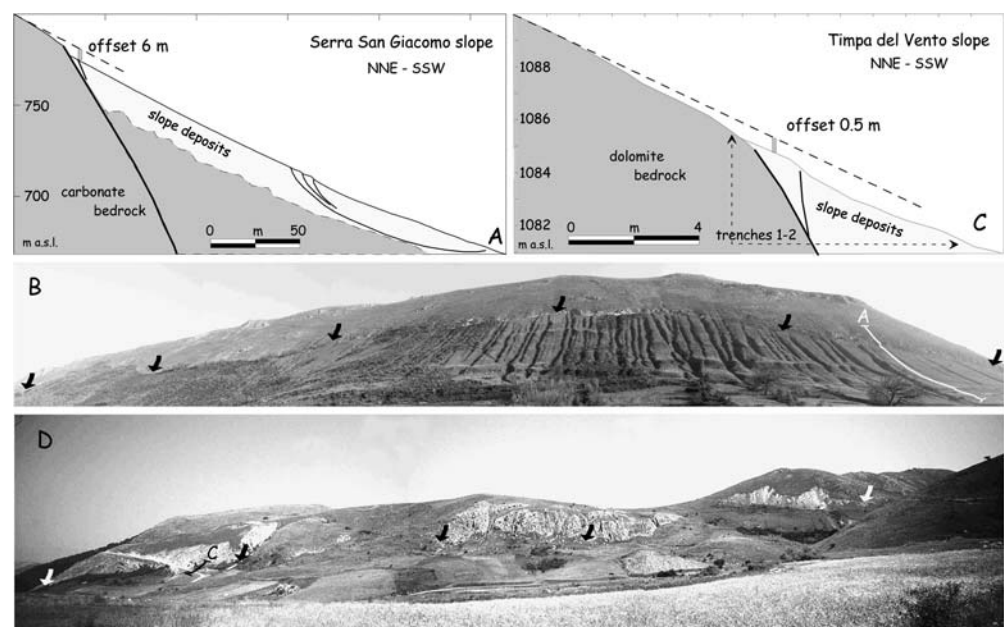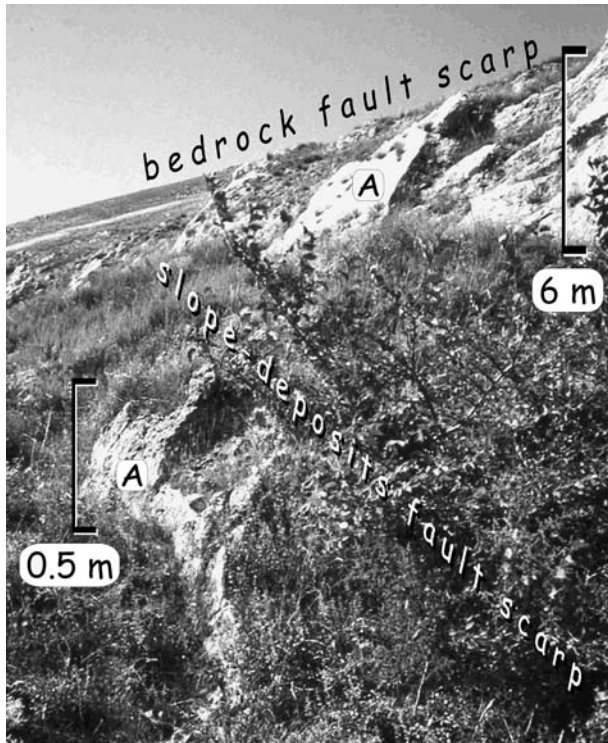
Fig. 5 Mt. San Giacomo fault scarp (*background*), close to the topographical profile traced on Fig. 4b. The ~post-18-ky slope deposits are affected by decimetric offset along secondary splays of the main fault (*foreground*). *A* polished fault plane

deposition of the Auletta conglomerates formation (lower Pleistocene?). In agreement with this interpretation, we found sparse Auletta conglomerates "hanged" along the Mt. San Giacomo crest.

In the hanging wall, stratified slope carbonate gravels (*grèze litée*, *sensu* Guillien 1951) are fault-dragged all along the length of the fault. They are well-sorted, centimetric, partially "open-work" (*sensu* Wasson 1979) gravels, being cemented only in the few decimeters under the ground surface. In the northwestern part of Mt. San Giacomo, where the fault reaches the base of the hillslope, the slope deposits are generally finer and matrix supported and consist of reddish sands with abundant carbonate, angular fine gravel, with indurated calishes. As for the age of these sediments, which we interpret as climatogenic slope-deposits (cold period), a ^{14}C radiocarbon dating provided a time span of 16730–15900 BP (sample MSJ-1, 2σ calibrated age; oldest Dryas?). In the sector of the fault scarp characterized by NE convexity (eastern tip), slope deposits are affected by decimetric offsets across secondary fault planes, which "rectify" the fault trend (Fig. 5). On the fault plane, *striae* show dip-slip or sinistral oblique motion (pitch <70°). A 300-m-long, 1-m-spaced topographical profile carried out along the southern slope of Mt. San Giacomo (Fig. 3) provided a quantitative amount of the fault scarp height (Fig. 4a). Assuming as elsewhere in the carbonate Apennine (Dramis 1983) that the formation of slope

rectilinear profiles took place during the long cold and arid climatic phase following the last glacial maximum (LGM; 25–21 ky BP), the measured ~6 m offset of the slope profile could be almost entirely attributed to post-16 ky (age of the last cold climate-related slope deposits). In other words, erosion and sedimentation rates before 16 ky were higher than fault throw-rates, so fault scarps were degraded or buried quickly (see also Roberts and Michetti 2004). Southward of Mt. San Giacomo, the fault continues through the Miocene arenaceous, and marly units which surround the prominent carbonate spur of Caggiano. Here, its surficial expression is almost entirely erased by vast landslides and soil creeps, and by the anthropic terraces, which characterize the whole hillslope. However, its "geological" evidence (i.e., tectonic contact between the Jurassic limestone and flyschoid terrain) has been found south of Caggiano during the driving of a tunnel (see location in Fig. 3).

Differently from the Timpe fault, the absence of colluvial and/or organic-rich deposits across the Monte San Giacomo fault scarp yielded the inutility of trenching this sector of the fault for paleoseismic purpose.

Timpe fault

The southwest-facing, 8-km-long Timpe fault scarp was identified firstly on a shaded digital elevation model derived from Istituto Geografico Militare (IGM) data (20-m data spacing, Fig. 3, inset a) and then checked and mapped through aerial photos and field survey. It partly fits with a rectilinear fault mapped by Scandone and Bonardi (1968) between Triassic and Miocene rocks, being recognized and interpreted in terms of active tectonics by Cello et al. (2003) and Galli and Bosi (2003b). It can be discontinuously followed along the southwestern slopes of Mt. Capo la Serra, Timpa del Vento, Timpa dell'Arpa (Timpe in Fig. 3), and Mt. Sierio, as a net fault scarp in the dolomite bedrock, while it is faintly visible in the hill slope sectors subject to the landslides which characterize the Miocene clayey units (Fig. 4d). In the Timpa del Vento hills slope, low-elevation air photos (2,600 m a.s.l., 1980s IGM fly) show the presence of a scarplet affecting a presently active decametric alluvial fan. We carried out a 20-m-long, 0.5-m-spaced topographical profile along the fan, which provided the amount of the scarp height (0.5 m, c in Fig. 4d). On the whole, the fault borders two narrow (200–400 m), intermontane basins (Timpa del Vento and Campo di Venere basins, TB and VB in Fig. 3), divided by a bedrock saddle. Both basins are flat and overflooded close to the natural outlet, their drainage being dammed by the uprising footwall. Moreover, downstream the fault, the *talweg* of the effluents is deeply entrenched in the carbonate bedrock, possibly evidencing the competition between remounting erosion and tectonic coseismic damming. Actually, in the Timpa del Vento basin, the reclamation of the
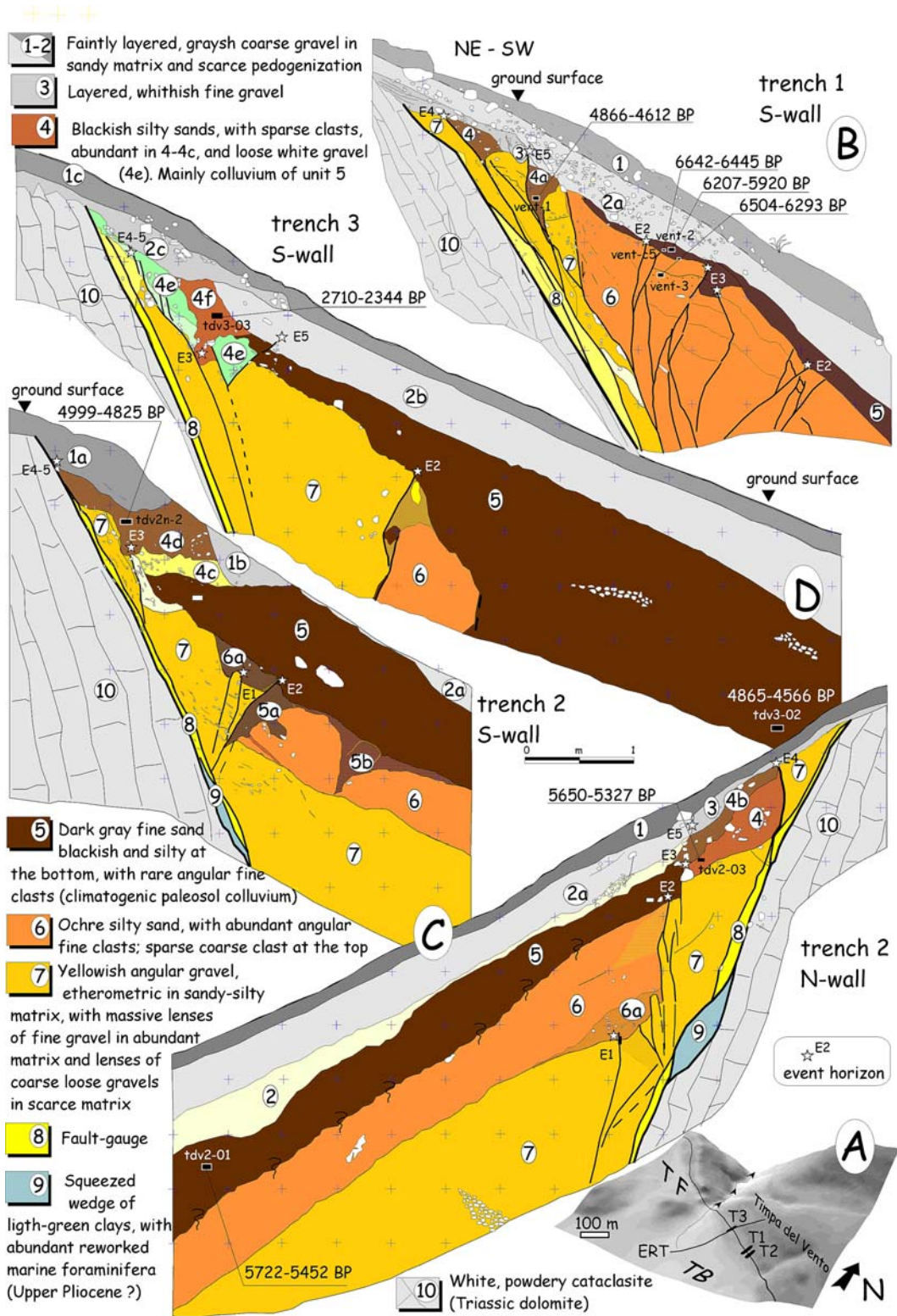
Fig. 6 a 3D shaded relief map showing the location of the trenches (*TF* Timpe fault, *TB* Timpe basin, *ERT*, electrical resistivity tomography profile. *Arrows* indicate the entrenched stream in the footwall). **b–d** Sketches of the southern wall of the three trenches excavated across the Timpa del Vento fault (northern wall of trench 2 is shown in the *bottom*). Faulting events and stratigraphy are discussed in the text

Table 3 Laboratory and calibrated radiocarbon ages of material sampled in trenches 1–3

	Sample	Unit	Analysis	Dated material	Conventional radiocarbon age (year BP)	Calibrated BP age range (1σ−68%)	Area (%)	Calibrated BP age range (2σ–95%)	Area (%)
Trench 1	VENT-1	4a	R, BLC	Organic silt	4230 ± 50	4851–4809	38	4866–4784	35
						4759–4703	47	4768–4612	62
						4671–4650	15		
	VENT-2	6–5	R, BLC	Organic silt	5300 ± 80	6173–6128	23	6207–5920	92
						6120–5988	69		
	VENT-3	6	R, BLC	Organic silt	5630 ± 60	6450–6387	51	6504–6293	96
						6372–6312	44		
	VENT-C5	6–5	AMS	Charcoal	5750 ± 40	6623–6604	15	6642–6445	98
						6604–6584	15		
						6569–6491	70		
Trench 2	TDV2-01	5	R, BLC	Organic silt	4840 ± 70	5652–5574	56	5722–5452	94
						5538–5474	44		
	TDV2-03	4	R, BLC	Organic silt	4800 ± 60	5599–5567	26	5650–5449	88
						5557–5470	74	5383–5327	12
	TDV2N-02	4d	R, BLC	Organic silt	4320 ± 50	4964–4928	32	4999–4825	94
						4913–4899	11		
						4881–4833	58		
Trench 3	TDV3-02	5	R, BLC	Organic silt	4200 ± 70	4835–4791	23	4865–4566	96
						4764–4621	77		
	TDV3-03	4f	R, BLC	Organic silt	2410 ± 50	2705–2666	18	2710–2628	24
						2472–2350	75	2514–2344	64
	MSJ-01	–	AMS	Organic sediment	13560 ± 80	16650–15980	68	16730–15900	95

R radiometric standard analysis, *BLC* bulk low carbon, *AMS* accelerator mass spectrometry. Calibration according to Stuiver et al. (2003)

plain for agricultural purpose was made possible in the past by excavating a 2 m deep canal across the fault zone. Available logs of wells drilled in the 1980s in this basin (CMT 1988), show at the top the presence of up to 3–4 m of sandy clay, with fine carbonate clasts, and argillified volcanic ashes. This level, overlapping the uppermost slope debris levels, could represent the last episodes of marsh environment, related to the fault-controlled damming of the basin. On the other hand, the lower portion of the well-logs shows (above the limestone bedrock) 15 m of yellowish sandy clay and gray-blue clay, rich in macrofossils, that we relate to remnant of the marine Pliocene transgression deposits [upper Pliocene coastal deposits, according to Lucchetti (1943); now raised over 1,100 m a.s.l.], preserved from aerial erosion by the sinking of the basin.

Paleoseismic analyses along the Caggiano fault

In June 2002, we opened a first 5-m-long, 3-m-deep trench across the Timpe fault scarp (trench 1, Fig. 6b, see location in Fig. 6a). This test site highlighted the presence of faulted late Holocene colluvial and slope-derived deposits (^{14}C dating), in tectonic contact with dolomite rocks. Thus, in May 2003 we opened two other trenches along the fault scarp (trenches 2–3, respectively, 7 m long, 3 m deep, and 8 m long, 3 m deep; Fig. 6c, d) in the geologically most favorable area (Timpa del Vento basin). Apart from the presence of a net fault scarp affecting both the bedrock and alluvia (i.e., fan) and colluvial/detrital deposits (suitable for paleoseismic purposes), this median sector of the fault is the one characterized by the highest geological offsets all along the entire CF (see also Cello et al. 2003).

We dated stratigraphic units through ^{14}C analysis. Samples were sent to Beta Analytic Inc. (Miami, USA) for absolute dating. Table 3 summarizes the accelerator mass spectrometer (AMS) and radiometric (R) ^{14}C analyses of sampled detrital charcoal and soil/deposit bulk. When possible, we preferred to date charcoals selected amongst the largest, most angular, apparently least decayed fragments, in order to minimize the chance of analyzing reworked carbon older than the host sediment. Samples yielded a variety of ages, ranging from 2410 ± 50 radiocarbon year BP to 5750 ± 40 years BP. Conventional ages have been calibrated using program Calib 4.1 (Stuiver et al. 2003); relative 1σ (68%) and 2σ (95%) areas under probability distribution are shown on the right columns in Table 3, together with the associated value for each age subinterval. In the text as in trench logs, samples have been reported with 2σ calibrated age (in case of multiple intervals, we adopted the whole 2σ range).

Stratigraphy of the faulted succession

The data gathered in the three trenches and the geological and geophysical survey performed in their near field allowed the definition and the chronological constrain of the faulted succession. Apart from the Triassic dolomite footwall (unit 10 in Fig. 6) and slices of upper Pliocene clays squeezed along the fault plane (unit 9 in Fig. 6), the exposed detrital/colluvial deposits range in age between ~7 ky and ~present. In a crude distinction between

detrital and colluvial units (which sometime fade into one other, the one being the colluvium of the other; e.g., units 6 and 7), one could subdivide the former in alluvial fan deposits (units 1, 1a, 1b, 2, 2a; limited to trenches 1 and 2 area) and slope deposits (1c, 3, 8, "open work;" 7, matrix supported). The colluvial units are, instead, represented by units 5 and 6, and, locally, by unit 4. In particular, while unit 4 is fault-generated colluvia of unit 5 and others, unit 5 is an areal deposit mantling the slopes of the basin, i.e., it is partly the climatogenic product of soils dismantling in the footwall.

The comparison within and among the correlative units in the three trenches suggests that the obtained absolute ages of samples do not always account for the depositional age of hosting sediments, being possibly older than the unit itself. This is due to the colluvial nature of sediments (i.e., dating the bulk of a colluvium we obtain partly the age of its parent, older material) and to the presence of charcoals burned, eventually, hundreds of years before their burying (see Nelson et al. 2003 and reference therein).

Unit 9 (Fig. 6c) is a slice of light-grayish clay trapped and dragged along the fault. It contains abundant traces of reworked upper Cretaceous–Paleocene foraminifera (determination, courtesy of R. Pichezzi, Geological Survey of Italy), and it should represent the Pliocene clays, which have been found in the previously mentioned boreholes.

Unit 7 (Fig. 6b–d) is the oldest deposit outcropping in all trenches (unit 8 is a tongue of loose dolomite clasts in silty-clayey matrix, dragged along the fault). It is mainly composed of yellowish gravels with etherometric, angular clasts ($\Phi_{max} = 5$ cm), in sandy–silty matrix. It contains both lenses of massive, fine gravels in abundant matrix and of coarse, loose gravels in scarce matrix. It is stratigraphically overlaid by unit 6, or truncated by an erosion surface visible under unit 5. No absolute dating was possible in this unit; thus, it must considered older than 6530–6300 BP (unit 6) and possibly related to one of the cold and arid climate phases following the LGM [Galli et al. (2005) have found very similar deposits in

Fig. 7 Electrical resistivity tomography carried out in the Timpe basin across the Timpe Fault (see location in Fig. 3). a Wenner–Schlumberger configuration: the 1-m-electrode-spaced profile was carried out close to the trench 3 (d) site and shows clearly the contact between the Triassic dolomite (unit 10) and the wedge of slope deposits which grew against the fault. b Wenner–Schlumberger configuration: this 10-m-electrode-spaced profile shows the nail of slope deposits in the hanging wall and the geometry of the Timpe basin in depth. The top of the bedrock (calibrated by means of boreholes) is slightly tilted against the fault. c Dipole–dipole configuration; 10-m-electrode-spaced profile showing the abrupt, tectonic contact between the dolomite and the Plio-Quaternary sediments (units labels as in Fig. 6)
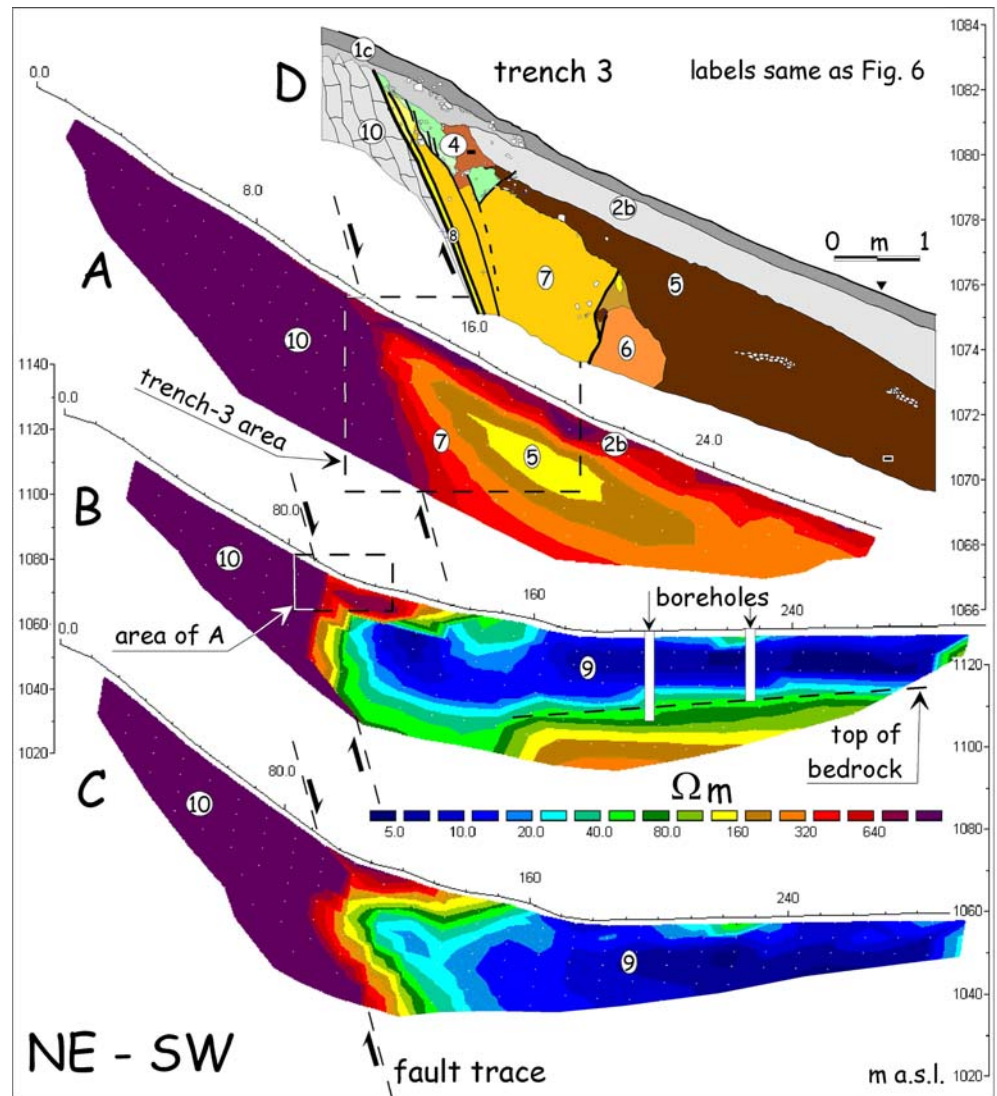
central Apennine, the age of which is post-date by 8040–7840 BP].

Unit 6 is faintly layered, orange silty sands, with abundant fine angular clasts ($\Phi_{max} = 1$ cm), and rare sparse coarse clasts at the top ($\Phi_{max} = 10$ cm). We found only one large angular charcoal (VENT-C5) at the interface between units 5 and 6, which provided an age of 6642–6445 BP, while other two bulk samples picked at both the interface and inside unit 6 (VENTS-2 and -3), gave, respectively, 6207–5920 and 6504–6293 BP (Fig. 6b). Considering that the age of charcoals could be some hundred of years older than their hosting sediments (e.g., Gavin 2001), we can hypothesize that the end of deposition of unit 6 is contained roughly within the sixth millennium BP.

Unit 5 is a blackish, silty–sandy, organic colluvium, grayish in its upper part, with rare, subangular, fine clasts ($\Phi_{max} = 1$ cm). It mantles everywhere the underlaying units, reaching its maximum thickness (> 2 m) in trench three. We obtained several ^{14}C ages for this unit (Table 3), the youngest being 4865–4566 BP (bulk sampled in the lower most part of trench three; TDV3-02). Considering the thickness and homogeneity of unit 5, the parent material from which it colluviated should have been an extended and thick paleosoil, no more existing in the footwall (i.e., eroded and dismantled). Therefore, its depositional age could be younger than the one obtained from the dating of its bulk. Anyway, the end of its deposition was before the half of the fifth millennium BP.

Unit 4 is composed both by blackish, silty sands, with coarse sparse clasts (4, 4c) and loose gravels (4e). It outcrops only close to the fault zone, and it is being interpreted as fault-generated colluvium derived mainly from unit 5. The obtained ages are the same as unit 5, with the exception of unit 4f (trench 3; TDV3-03), which provided an age of 2710–2344 BP.

Unit 3 is fine-layered gravels, in scarce matrix. It appears only in a wedge limited between the main and a secondary fault. Units 1 and 2 are angular, coarse gravels ($\Phi = 1$–10 cm), in sandy, gray-brownish matrix, with a very low grade of pedogenization and with horizon A very thin (2 and 3 cm) or absent. As unit 3, these units are erosive on the underlaying deposits. Their age is analytically undeterminable, being, of course, younger than unit 4f (2710–2344 BP). The most important detrital production in the past two millennia in the Apennines has been related by Giraudi and Mussi (1999) to particular climate period (cold and arid), and in particular to the Little ice age (LIA; Lamb 1977), that is between the fifteenth and the nineteenth century A.D. Therefore, it is possible that at least unit 2 (unit 1 is somehow still in deposition) was mainly sedimented in that time.

Geophysical analyses

The overall geometry of the Timpa del Vento basin has been investigated also by means of 2D electrical resis-
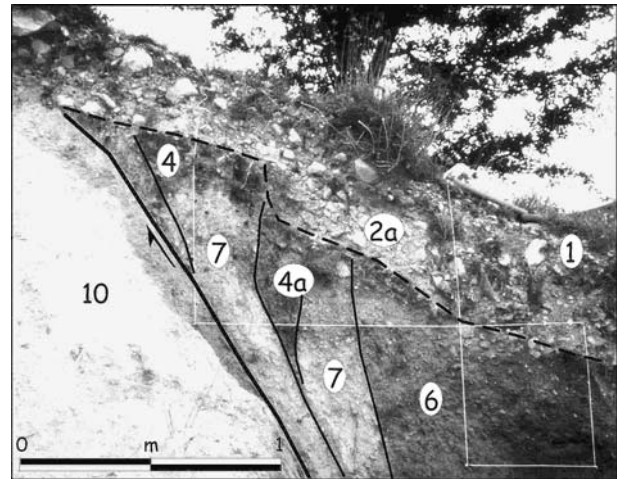

Fig. 8 View looking SE of the upper part of trench 1 during the excavation phases. Units labeled as in Fig. 6. Units 4–7 containing Late Holocene-historical age dates, being faulted against the Triassic dolomite (10) of the Timpe-Mt. Sierio range. Unit 2, which is possibly of modern age, might contain 1 and 2 surface ruptures events

tivity tomography (ERT), which has been compared and calibrated with well-logs and the stratigraphy of trenches. Profiles were carried out along the trace of trench three (Fig. 7).

The electrical imaging or ERT is a geoelectrical method, widely applied to obtain 2D and 3D high-resolution images of the resistivity subsurface patterns in areas of complex geology (Griffiths and Barker 1993; Sharma 1997; Dahlin 2001). It has been shown to be useful for mapping and characterizing the deep geometry of active faults (Giano et al. 2000a, b; Suzuki et al. 2000; Caputo et al. 2003). Technically an ERT survey can be carried out using different electrode configurations [dipole–dipole (DD), Wenner–Schlumberger (WS), etc.] that are dislocated on earth surface to send into the ground the electric currents and to measure the generated voltage signals (for details about our field procedure see Caputo et al. 2003 and references therein). In this work, we used both DD and the WS configuration, the latter considered as having a good signal response, the ability to resolve horizontal and vertical structures relatively well, and a good depth of investigation (Loke 2001).

Resistivity field data were collected with a Syscal R2 earth resistivity meter of the Iris instruments and a 32-electrode cable with an electrode spacing ranging from 2 to 10 m. The Res2dinv resistivity inversion software (Loke 2001) was used to automatically invert the apparent resistivity data from the field. The inversion routine is based on the smoothness constrained least-squares inversion (Sasaki 1992) implemented by using a quasi-Newton optimization technique. The subsurface is divided into rectangular blocks, the number of which corresponds to the number of measurement points. The optimization method adjusts the 2D resistivity model trying to iteratively reduce the difference between the calculated and measured apparent resistivity values. The

root-mean-squared (RMS) error provides a measurement of this difference (Loke 2001). In particular, due to the expected sharp resistivity boundaries between the carbonate bedrock and the sandy–clayey sediments of the basin, a robust inversion method was applied. This method minimizes the absolute difference between the measured and calculated apparent resistivity values (Loke 2001).

Figure 7 shows the inverse model resistivity sections related to three among several electrical tomographies carried out across the Timpe fault. The analysis of the obtained electrical images allows us to identify strong variabilities of electrical resistivity values, from about 5 Ω m (sandy–clayey material; unit 9 of Figs. 6, 7) to more than 1,000 Ω m (carbonate bedrock; unit 10), with the occurrence of a strong step in the resistivity distribution fitting with the fault plane observed both in the paleoseismological trenches and in the field.

The results gathered through the DD method (10 m electrode spacing, 310-m-long section; Fig. 7c) evidence clearly the dip of the fault in depth ($\sim$75°), the wedge of slope debris, and colluvia from the fault tapers downslope (dark body with resistivity >160 Ω m). This feature is specifically highlighted in Fig. 7a by the WS 2-m-electrode spacing section (31 m long), which shows the debris and colluvial wedge growth against the fault plane. The different resistivity levels account for the stratigraphical units visible in trench 3 (Fig. 7d) and described in the following chapter. The WS profile shown in Fig. 7b (10 m electrode spacing, 310-m-long section), apart from the fault trend in depth and the debris nail deposited in the hanging wall, highlights a possible gentle tilting of the carbonate bedrock top surface toward the fault in the hanging wall itself. Finally, the low resistivity body (<30 Ω m), corresponding to the Pliocene sandy clay found in boreholes (unit 9 in Figs. 6, 7), shows an upward dragging as approaching the fault. In fact, slice of squeezed gray clay has been found packed along the fault plane in the trenches, at an elevation of at least 20 m above the Pliocene sediments in the basin.

As expected, the ERT with 2-m electrode spacing gives a more detailed resolution, especially in the upper most levels, and a shallower investigated depth. Conversely, the 10-m electrode spacing shows a poorer general resolution but a deeper investigated depth. This is particularly evident considering the difference between the resistivity values of the slope debris/colluvial units in the 2-m versus the 10-m electrode spacing ERT ($\rho > 150$ Ω m, and $\rho > 320$ Ω m, respectively).

Trench 1

This trench is located across the "scarplet" visible on 1980 aerial photos (IGM fly). As aforementioned, this scarp affects a small active alluvial fan, the down-flow of which has been now artificially canalized. The trench was excavated in the northern side of the fan-lobe, its length being limited SW by the cut of a dirty road. All units exposed in the trench wall, with the exception of unit 1 (Figs. 6b, 7, 8), are faulted. The footwall is composed by white, powdery cataclasite (Triassic dolomite; unit 10), exhibiting a polished fault plane (N110°, 58°), which separates unit 10 from the slope detrital succession. Striae on the plane have a pitch of 110° (i.e., roughly dip-slip, with dextral component).

Units 6–8 contains at least one event (E2; an oldest visible event, E1, is not present in this trench) occurred before the deposition of unit 5, the latter sealing some splays of the fault. Then, two different splays cut through unit 5, testifying a successive faulting event (E3). If, as interpreted, unit 4 is colluvia of unit 5 (possibly remains of a colluvial wedge originated from unit 5 after E3), they have been successively faulted (E4) and sealed by unit 3. Finally, unit 2 shows a thickening downward of unit 3, with a small wedge of gravels, which in-fills the step formed between the fault that separates units 3, 8 from 2, 4a. This thickening could be an effect of E4, or it could be representative for an ultimate event, occurred during, or slightly before the deposition of unit 2 (E5).

Trench 2

This trench is located 10 m SE to the former, across the same scarplet in the alluvial fan. Similarly to trench 1, all units apart from unit 1 are faulted (Fig. 6c). In the fault gauge a slice of Pliocene (?), light-grayish clay is packed between the dolomite and the slope succession. Unit 7 contains one event (E1; Fig. 6c, N-wall), occurred before the deposition of unit 6. The latter, in fact, seals some secondary splay of the fault and presents, at the base, a wedge of chaotic gravels (unit 6a, colluvial wedge related to E1?). Unit 6 is then faulted against unit 7 (E2) before the deposition of unit 5. After its deposition, unit 5 is also faulted against unit 7 (E3), and partly covered by its own fault-generated colluvia (unit 4). Unit 4 has been then clearly faulted against unit 7 by a successive event (E4), and sealed by unit 3. Finally, also here the thickening of unit 2 might testify the formation of a fault scarp, providing a possible evidence for a further event (E5).

Trench 3

This trench was excavated $\sim$100 m NW to trench 1, outside the area affected by the alluvial fan (Fig. 6d). Similarly to trenches 1 and 2 it shows the existence of at least one event before the deposition of unit 5, which faults unit 6 against unit 7 (E2). Unit 5 is partly overlapped by its own fault-generated (?) colluvium (unit 4; E3?). The latter is then faulted against units 7, 8 and 10, being sealed by unit 2c (E4). Analogously to the other trenches, the deposition of unit 2a, which is slightly offset by a secondary fault, is supposed to represent the

slope response to the formation of a fault scarp (E5) occurred during the deposition of the units itself.

Discussion

The paleoseismological analyses carried out along the CF demonstrate that this fault experienced repeated surface faulting events in the past seven millennia. One of the most important issues concerning the present activity of the CF is that it is located between the MFS at NW and the debated seismogenic structure responsible for the 1857 mainshock in the Agri valley at SE (Fig. 2). Its northern tip overlaps (through a right step of 5 km) the southern tip of the MFS (i.e., San Gregorio Magno fault). Although dipping in opposite directions, both these faults account for the same NE–SW extensional regime, the same provided by the SW-facing Ufita fault (Brancaccio et al. 1981; Fig. 2a), located north of the MMF. This is in agreement with the observation that in the southern Appenine chain, available stress indicators (e.g., breakout data, focal mechanism) show a very uniform NE–SW S_{hmin} direction (Montone et al. 1999). The seismogenetic characteristics of the CF deduced from our analyses can be summarized as follows.

Paleoearthquakes

Considering the significance of the ^{14}C age obtained for the different units, that is their weak chronological constrains, we choose to suggest only tentative, rough event-windows. The oldest identified event (E1, present only in trench 2) occurred before (and partly generated) the deposition of unit 6a–6, the top of which sedimented not later than the second half of the seventh millennium BP. E2, visible in all trenches as cutting through unit 6, but being sealed by unit 5, occurred between the end of the seventh millennium BP, and, at least, the half of the fifth millennium. E3 might have occurred during or at the end of the sedimentation of unit 5, faulting this unit against older ones, and generating erosion and colluvia (unit 4) from its correlative beds in the footwall. The age of E3 is much younger than the second half of the fifth millennium, and could be roughly indicated by the younger age of its colluvial deposit (unit 4, half of the third millennium BP, if true). E4 and, eventually, E5 fault unit 4 against older units, being, therefore, younger than the second half of the third millennium BP (i.e., 2720–2340 BP). As a working hypothesis, if it was true that unit 2a sedimented after or during the formation of a fault scarp (actually, in trenches 1 and 3 its bottom is faulted), and if this unit is related to the cold and arid phase recorded elsewhere during the LIA, then, E5 and/or E4 might have occurred during the fifteenth and nineteenth century A.D. Considering the historical earthquake capable to produce surface faulting in the area, one should not exclude that the 1561 event and/or the northern shock of the 1857 event might be generated by the CF.

Recurrence time

It is not possible to provide reliable earthquake return period for the CF, because of the amplitude of the event windows and the uncertainness of depositional ages. Moreover, time return relative to a single fault may vary in condition of stress triggering (Nostro et al. 1997) due to activation of neighboring fault (e.g., Galli et al. 2005). Anyway, assuming E1 to be occurred before 7 ky BP, the average recurrence of surface faulting event could be 1.6 ky. This value is consistent with others paleoseismologically derived data along the axial belt of the Apennine (i.e., 1–3 ky; e.g., in central Apennine: Norcia fault, Galli et al. 2005; Ovindoli-Pezza fault, Pantosti et al. 1996; Fucino fault, Galadini and Galli 1999; e.g., in southern Apennine: N-Matese fault, Galli and Galadini 2003; Mt. Marzano fault, Pantosti et al. 1993; e.g., in Calabria: Mt. Pollino fault, Cinti et al. 2002; Lakes fault, Galli and Bosi 2003a; Cittanova fault, Galli and Bosi 2002).

Slip rates and offsets

Although there are no correlative beds across the main fault, we have some indications concerning the slip rate of the CF. The first one, averaged on a long period, derives from the topographical profile carried out along the Mt. San Giacomo slope (Fig. 4a). As mentioned before, if we relate the measured 6-m offset across the fault as due to cumulated ruptures occurred after the climatic flattening of the slope (ended ∼16 ky), we obtain a minimum slip rate of ∼0.4 mm/year. On the other hand, as far as the Timpe fault is concerned, assuming that the age of the bottom of unit 6 might be close to the seventh millennium BP, trench 2 shows a minimum offset of this level of 2.8 m (0.4 mm/year). Analogously, all trenches provide a minimum offset for the base of unit 5 of 1.4 m (assuming unit 5 eroded in the footwall), consistent with a minimum slip rate of 0.3 mm/year. In one case (trench 2), it was possible to measure the offset caused by E4 across the fault separating units 4–7 and sealed by unit 3. Although both erosive, the top of unit 7 across the fault is displaced (at least) by 0.7 m. Finally, if unit 2a represents the downhill filling of the E5-generated fault scarp, its average thickness would account for an offset of 0.4–0.5 m. In fact, this value fits with the height of the scarplet measured by means of the 0.5-m-spaced topographical profile (0.5 m; Fig. 4c) between trenches 1 and 2. An indirect confirmation of the same value comes from the ratio between assumed recurrence time and offset *per* event, that is 0.5 m/1.6 kyr = 0.3 mm/year.

Maximum associated magnitude

Considering different empirical relationships among surface rupture and magnitude (e.g., Wells and Cop-

persmith 1994; Ambraseys and Jackson 1998), and assuming coseismic offsets of ∼0.5 m, the surface length of the CF (∼17 km) would account for $M_s \approx 6.6$. A slightly different value ($M_w = 6.3$) can be obtained evaluating the magnitude from the seismic moment potentially attributable to the fault (i.e., $M_o = Adu$, where A is fault area; d, offset; u, rigidity modulus assumed to be 3×10^{11} dyn cm and seismogenetic thickness of ∼15 km; then, $M_w = \log M_o / 1.5 - 10.73$). Obviously, we do not exclude the possibility that the two strands of the CF, namely the Mt. San Giacomo and Timpe faults, may rupture separately. In this case regression curves offer an estimate of $M_s \approx 6.3$, while $M_w \approx 6.1$ is obtained through the seismic moment evaluation (considered offset of 0.3 m; Wells and Coppersmith 1994).

Associated historical earthquakes

The paleoseismic analysis shows the presence of 1 and 2 events (E4–5) occurred after 2720–2340 BP, and, preferentially, during/after the LIA (fifteenth and the nineteenth century A.D.). While we ignore the historical seismicity preceding the year 1000, we are confident that at least one earthquake in the past millennium had its epicenter close to the CF. This is the 1561 earthquake, the equivalent macroseismic magnitude of which ($M_e = 6.6$) is in the same order of the analytically derived magnitudes associated to the CF. We have discussed about the two main shocks of the 1561 sequence; an attractive hypothesis, which makes no claim to being conclusive, is that the shocks of July 31, and August 19 were generated by the two strands of the CF, the latter triggered by the former. The cumulated effects of the two $M_s \approx 6.3$ events would account for the evaluated $M_e = 6.6$. Moreover, at least the Timpe segment could be eventually responsible for the strong foreshock (Baratta 1901; Magri and Molin 1979), which preceded the December 16, 1857 earthquake (see Branno et al. 1983; Cello et al. 2003).

Conclusions

We took both a geological and historical approach to the definition and characterization of the CF, a previously poorly known N120° normal fault, which borders the NE slopes of the Maddalena Mts. (southern Apennines). The CF is composed by two main en echelon strands, separated by a 1-km right step (Mt. San Giacomo and Timpe faults). The southern branch has been investigated by means of ERT and of three paleoseismological trenches, which showed the surface ruptures history of the fault for the past 7 ky. Vertical slip rates evaluated both by means of topographical profiles on morphotectonic elements, and across the faults exposed in trenches yielded a minimum value of 0.3–0.4 mm/year. This value is in the same order of the other known active faults of the Apenninic chain.

Although our feeling is that the absolute dating (^{14}C) of the samples does not constrain conclusively the age of the hosting deposits, a possible *suite* of four-five surface faulting events (E1–5) seems to affect the slope units in trenches. E1 occurred slightly (?) before ∼7 ky BP, E2 is confined roughly between 6.5 and 4.5 ky BP, E3 roughly between ∼4.5 and 2.5 ky BP, E4–5 after 2.5 ky BP, and eventually during/after the fifteenth and nineteenth century A.D. Thus, similarly to other Apenninic faults, the average recurrence time of CF could be in the order of 1.6 ky, unless the presence of time-clustered events (e.g., E4–5). As far as any correlation with the historical seismicity is concerned, we observed that the $M_e = 6.6$, 1561 earthquakes (July 31 and August 19; cumulated equivalent magnitude) had their mesoseismic area around the CF. Thus, one could reasonably hypothesize that the two shocks (or at least the easternmost) were generated by the two CF branches (each one capable to generate $M_s \approx 6.3$), the latter being eventually triggered by the former. Finally, also the strong foreshock of the 1857 event struck the villages located in the northern mesoseismic area, close to the Timpe fault. In agreement with Cello et al. (2003), E5 could be related to this event.

From the geometrical and kinematic point of view, the CF could represent the *trait d'union* between the known $M_e = 6.5$, 1466 and $M_s = 6.9$, 1980 EQ fault (MFS) and the still debated seismogenetic structure responsible for the main, catastrophic 1857 shock in the Agri Valley ($M_e = 7$). Similarly to the MFS, although dipping oppositely, the CF accounts for the current NE–SW extension in the Apennines.

From all the above, it seems that both the MFS and CF are not characterized by regular recurrence time. If it is true that the former ruptured in 1466 and again in 1980, and the latter in 1561 and again in 1857, their last rupture intervals are much shorter (0.5 and 0.3 ky, respectively) than their average recurrence (>1.5 ky). A similar behavior has been recognized in central Italy only in the N-Matese fault, which ruptured in 1456 and 1805, after >1.7 of "silence" (i.e., ∼280 B.C.: Galli and Galadini 2003).

The identification of CF and the seismogenetic characterization of both CF and MFS fill another small gap in the knowledge of seismotectonics of southern Apennines, providing new data useful for hybrid probabilistic seismic hazard assessment (PSHA; e.g., Peruzza et al. 1999; Bosi and Galli 2004).

References

Amato A, Selvaggi G (1993) Aftershock location and P-velocity structure in the epicentral region of the 1980 Irpinia earthquake. Ann Geofis 36:3–15

Ambraseys NN, Jackson JA (1998) Faulting associated with historical and recent earthquakes in the Eastern Mediterranean region. Geophys J Int 133:390–406

Ascione A, Cinque A, Tozzi M (1992) La valle del Tanagro (Campania): una depressione strutturale ad evoluzione complessa. St Geol Cam special issue (1):209–219

Baratta M (1901) I terremoti d'Italia. Saggio di storia, geografia e bibliografia sismica italiana, Torino, pp 1–950

Basso C, Di Nocera S, Matano F, Totte M (1996) Evoluzione geomorfologica ed ambientale tra il Pleistocene superiore e l'Olocene dell'area tra Castelbaronia e Vallata nell'alta valle del fiume Ufita (Irpinia, Italia meridionale). Il Quaternario 9:513–520

Benedetti L, Tapponier P, King G, Piccardi L (1998) Surface rupture of the 1857 southern Italian earthquake. Terra Nova 10:206–210

Bernard P, Zollo A (1989) The Irpinia (Italy) 1980 earthquake: detailed analysis of a complex normal faulting. J Geophys Res 94:1631–1647

Bonito M (1691) Terra Tremante, o vero continuatione de' terremoti dalla creazione del mondo sino al tempo presente. Napoli, pp 1–822

Boschi E, Pantosti D, Slejko D, Stucchi M, Valensise G (eds) (1993) Irpinia dieci anni dopo, Special Issue, Ann Geofis 36:1–351

Boschi E, Guidoboni E, Ferrari G, Valensise G, Gasperini P (eds) (1997) Catalogo dei Forti Terremoti in Italia dal 461 a.C. al 1990. ING e SGA, Bologna, pp 1–644

Bosi V, Galli P (2004) Incorporating paleoseismological data in PSHA: the case of Calabria (southern Italy). Boll Geof Teor Appl 45:255–270

Brancaccio L, Cinque A, Sgrosso I (1978) L'analisi morfologica dei versanti come strumento per la ricostruzione degli eventi neotettonici. Mem Soc Geol It 19:621–626

Brancaccio L, Cinque A, Scarpa R, Sgrosso I (1981) Evoluzione neotettonica e sismicità in penisola sorrentina e in Baronia (Campania). Rend Soc Geol It 4:145–149

Branno A, Esposito E, Marturano A, Porfido S, Rinaldis V (1983) Studio su base macrosismica del terremoto della Basilicata del 16 dicembre 1857. Boll Soc Natur Napoli 92:249–338

Camassi R, Stucchi M (eds) (1996) NT4.1.1 a parametric catalogue of damaging earthquakes in the Italian area, http://www.emidius.mi.ingv.it/NT/home.html

Caputo R, Piscitelli S, Oliveto A, Rizzo E, Lapenna V (2003) The use of electrical resistivity tomographies in active tectonic: examples from the Tyrnavos Basin, Greece. J Geodyn 36:19–35

Castelli V (2003) Strong earthquakes included by chance in Italian catalogues: single cases or a hint of more? Ann Geophys 46:1247–1263

Cello G, Tondi E, Micarelli L, Mattioni L (2003) Active tectonics and earthquake sources in the epicentral area of the 1857 Basilicata earthquake (southern Italy). J Geodyn 36:37–50

Cinque A, Lambiase S, Sgrosso I (1981) Su due faglie nell'alta valle del Sele legate al terremoto del 23.11.1981, Rend. Soc Geol 4:127–129

Cinque A, Patacca E, Scandone P, Tozzi M (1993) Quaternary kinematic evolution of the Southern Appennenes. Relationships between surface geological features and deep lithospheric structures. Ann Geofis 36:249–260

Cinti FR, Moro M, Pantosti D, Cucci L, D'Addezio G (2002) New constraints on the seismic history of the Castrovillari fault in the Pollino gap (Calabria, southern Italy). J Seismol 6:199–217

CMT (Comunità Montana Tanagro) (1988) Progetto dei lavori di costruzione di invaso collinare in località Serra Cardone del comune di Caggiano, Relazione Geologica, pp 1-113 unpublished relation

Corpus Chronicorum Bononiensium (1940) In: Sorbelli A (ed) Rerum Italicarum scriptores, XVIII/I, Città di Castello 1910–1940

Dahlin T (2001) The development of DC resistivity imaging techniques. Comput Geosci 27:1019–1029

Devoti R, Ferraro C, Gueguen E, Lanotte R, Luceri V, Nardi A, Pacione R, Rutigliano P, Sciarretta C, Vespe F (2002) Geodetic control on recent tectonic movements in the central Mediterranean area. Tectonophysics 346:151–167

Dramis F (1983) Morfogenesi di versante nel Pleistocene superiore in Italia: I depositi detritici stratificati. Geogr Fis Dinam Quat 6:180–182

Figliuolo B, Maturano A (1996) Il terremoto del 1466. Rassegna Storica Salernitana 25:93–109

Frepoli A, Amato A (2000) Fault plane solution of crustal earthquakes in southern Italy (1989–1995): seismotectonics implications. Ann Geofis 43:437–467

Galadini F, Galli P (1999) The Holocene paleoearthquakes on the 1915 Avezzano earthquake faults (central Italy): implications for active tectonics in Central Apennines. Tectonophysics 308:143–170

Galadini F, Galli P (2000) Active tectonics in the central Apennines (Italy). Input data for seismic hazard assessment. Nat Haz 22:202–223

Galli P (2003) Two poorly known earthquakes of southern Campania, DPC—Seismic Survey of Italy, RT/SSN/03/01, pp 1–22 (in Italian)

Galli P, Bosi V (2002) Paleoseismology along the Cittanova fault. Implications for seismotectonics and earthquake recurrence in Calabria (southern Italy). J Geophys Res 107, DOI 10.1029/2001JB000234

Galli P, Bosi V (2003a) Catastrophic 1638 earthquakes in Calabria (southern Italy). New insight from paleoseismological investigation. J Geophys Res 108:B1 DOI 10.1029/2002JB01713

Galli P, Bosi V (2003b) Analisi paleosismologiche lungo la faglia di Caggiano (Monti della Maddalena, Sa), Gruppo Nazionale di Geofisica della Terra Solida, extended abstract of the 22° National Congress, Rome, pp 106–108

Galli P, Galadini F (1999) Seismotectonic framework of the 1997–1998 Umbria-Marche (Central Italy) earthquakes. Seismol Res Lett 70:404–414

Galli P, Galadini F (2003) Disruptive earthquakes revealed by faulted archaeological relics in Samnium (Molise, southern Italy). Geophys Res Lett 30, DOI 10.1029/2002GL016456

Galli P, Galadini F, Calzoni F (2005) Surface faulting in Norcia (central Italy): a "paleoseismological perspective". Tectonophysics 403:117–130

Gasperini P (2002) The Boxer program, release 3.02 available at: http://www.ibogfs.df.unibo.it/user2/paolo/www/boxer/boxer.html

Gavin DG (2001) Estimation of inbuilt age in radiocarbon ages of soil charcoal for fire history studies. Radiocarbon 43:27–44

Giano S, Maschio L, Alessio M, Ferranti L, Improta S, Schiattarella M (2000a) Radiocarbon dating of active faulting in the Agri high valley, southern Italy. J Geodyn 29:371–386

Giano SI, Lapenna V, Piscitelli S, Schiattarella M (2000b) Electrical imaging and self-potential surveys to study the geological setting of the Quaternary slope deposits in the Agri high valley (Southern Italy). Ann Geofis 43:409–419

Giraudi C, Mussi M (1999) The central and southern Apennine (Italy) during OIS 3 and 2: the colonisation of a changing environment. In: INQUA Congress, European Late Pleistocene, isotopic stages 2 and 3, Durban, South Africa, pp 118–129

Griffiths DH, Barker RD (1993) Two-dimensional resistivity imaging and modelling in areas of complex geology. J Appl Geophys 29:211–226

Guillien Y (1951) Les grèze litée de Charente. Rev Geogr Pyrénées Sud-Ouest 22:124–162

Ippolito F, Argenio BD, Pescatore T, Scandone P (1975) Structural and tectonic framework of southern Apennine. In: Geology of Italy, The Earth S. Society of the Lybian Arab Republic, Tripoli, pp 317–328

Lamb HH (1977) Climate: present, past and future, vol 2, Metheun & Co., London

Loke MH (2001) Tutorial: 2-D and 3-D electrical imaging surveys. In: Course notes for USGS workshop "2-D and 3-D inversion and modeling of surface and borehole resistivity data", Storrs, CT, 13–16 March 2001

Lucchetti L (1943) Rinvenimento di un deposito pliocenico marino nella zona delle Murge Nere (S. Angelo le Fratte, PZ). Boll Soc It Geol 62:39–40

Magri G, Molin D (1979) Attività macrosismica in Basilicata, Campania e Puglia dal 1847 al 1861, CNEN, RT/AMB (79) 5, pp 104

Mallet R (1862) Great Neapolitan earthquake of 1857. The first principles of observational seismology. Chapman and Hall, London

Meletti C, Patacca E, Scandone P (2000) Construction of a seismotectonic model: the case of Italy. Pure Appl Geophys 157:11–35

Michetti A, Ferreli L, Serva L, Vittori E (1997) Geological evidence for strong historical earthquake in an aseismic region: the Pollino case (southern Italy). J Geodyn 24:67–86

Monachesi G, Stucchi M (eds) (1997) DOM an intensity database of damaging earthquakes in the Italian area, http://www.emidius.mi.ingv.it/DOM/home.html

Montone P, Amato A, Pondrelli S (1999) Active stress map of Italy. J Geophys Res 104:2595–2610

Mucciarelli M, Valenzise G, Gallipoli MR, Caputo R (1999) Reappraisal of a XVI century earthquake combining historical, geological and instrumental information. In: Papers and memoranda from the 1st WS of the ESC WG "Historical Seismology", Macerata, Italy, pp 64–67

Nelson AR, Johnson SY, Kelsey HM, Wells RE, Sherrod BL, Pezzopane SK, Bradley LA, Koehler RD, Bucknam RC (2003) Late Holocene earthquakes on the Toe Jam Hill fault, Seattle fault zone, Bainbridge Island, Washington. Geol Soc Am Bull 115:1388–1403

Nostro C, Cocco M, Belardinelli M (1997) Static stress changes in extensional regimes: an application to Southern Apennines (Italy). Bull Seismol Soc Am 87:234–248

Pacca C (1563) Discorso del terremoto, Library of the Società Napoletana di Storia Patria, Naples, Fondo sismico, p 7/A3

Pantosti D, Valensise L (1990) Faulting mechanism and complexity of the November 23, 1980 Campania-Basilicata earthquake. J Geophys Res 95:15319–15342

Pantosti D, D'Addezio G, Cinti FR (1993) Paleoseismological evidence of repeated large earthquakes along the 1980 Irpinia earthquake fault. Ann Geofis 36:321–330

Pantosti D, D'Addezio G, Cinti FR (1996) Paleoseismicity of the Ovindoli-Pezza fault (Central Italy): a history including a large, previously unrecorded earthquake in middle ages (860–1300 A.D.). J Geophys Res 101:5937–5959

Parsons AJ (1989) Hillslope form, Routledge, UK, pp 1–212

Patacca E, Scandone P (1989) Post-Tortonian mountain building in the Apennines: the role of the passive sinking of a relic lithospheric slab. In: Boriani A, Bonafede M, Piccardo GB, e Vai GB (eds) The lithosphere in Italy: advance in earth science research. Accademia Nazionale dei Lincei, Rome, pp 157–176

Patacca E, Scandone P (2004) The 1627 Gargano earthquake (southern Italy). Identification and characterization of the causative fault. J Seismol 8:259–273

Peruzza L, Pantosti D, Slejko D (1999) Testing a new hybrid approach to seismic hazard assessment: an application to the Calabrian Arc (southern Italy). Nat Haz 14:113–126

Pescatore T, Sgrosso I, Torre M (1970) Lineamenti di tettonica e sedimentazione nel Miocene dell'Appennino campano-lucano. Mem Soc Nat Napoli Supp Boll 78:337–408

Pieri P, Vitale G, Benedice P, Dogliosi C, Gallicchio S, Giano S, Loizzo R, Moretti M, Prosser G, Sabato L, Schiattarella M, Tramutoli M, Tropeano M (1997) Tettonica quaternaria nell'area bradano-ionica. Il Quaternario 10:535–542

Postpischl D (ed) (1985) Atlas of isoseismal maps of Italian earthquakes, vol 114, 2A. Quaderni de "La Ricerca Scientifica", pp 1–164

Roberts G, Michetti A (2004) Spatial and temporal variations in growth rates along active normal fault systems: an example from The Lazio–Abruzzo Apennines, central Italy. J Struct Geol 26:339–376

Roberts GP, Michetti AM, Cowie P, Morewood NC, Papanikolaou I (2003) Fault slip-rate variations during crustal-scale strain localisation, central Italy. Geophys Res Lett 29, DOI 10.1029/2001GL013529

Sasaki Y (1992) Resolution of resistivity tomography inferred from numerical simulation'. Geophys Prospecting 54:453–464

Scandone P, Bonardi G (1968) Synsedimentary tectonics controlling deposition of Mesozoic and Tertary carbonatic sequences of areas surrounding Vallo di Diano (southern Apennines). Mem Soc Geol It 7:1–10

Schiattarella M, Di Leo P, Benedice P, Giano S (2003) Quaternary uplift vs tectonic loading: a case study from the Lucanian Apennine, southern Italy. Quaternari Int 101–102:239–251

Sharma PV (1997) Environmental and engineering geophysics. Cambridge University Press, Cambridge

Stuiver M, Reimer PJ, Reimer R (2003) Program CALIB 4.3 http://www.depts.washington.edu/qil/calib/

Suzuki K, Toda S, Kusunoki K, Fujimitsu Y, Mogi T, Jomori A (2000) Case studies of electrical and electromagnetic methods applied to mapping active faults beneath the thick quaternary. Eng Geol 56:29–45

Vera e distinta relazione del terremoto accaduto in Napoli e parte del suo Regno il giorno 8 di settembre (1694) DA Parrino e C Cavallo, Napoli

Vitale D (ed) (1695) In: Notai Ariano, b.173, Archivio di Stato di Avellino

Wasson RJ (1979) Stratified debris slope deposits in the Hindu Kush, Pakistan. Zeitsch Geomorph 23:301–320

Wells D, Coppersmith K (1994) New empirical relationships among magnitude, rupture length, rupture width, rupture area and surface displacement. Bull Seismol Soc Am 84:974–1002

Westaway R (1996) Fault rupture geometry for the 1980 Irpinia earthquake: a working hypothesis. Ann Geofis 36:51–69

Westaway R, Jackson JA (1987) The earthquake of 1980 November 23 in Campania-Basilicata (southern Italy). Geophys J Astron Soc 90:375–443

Working Group CPTI (1999) Catalogo parametrico dei terremoti italiani, ING, GNDT, SGA, SSN, Bologna, pp 1–92

Young A (1972) Slopes. In: Oliver and Boyd (eds) Edinburgh